E-PLANE PATTERN OF THICK EDGE HORNS

by

Asoknath Chattopadhyay

Submitted in partial fulfillment
of the requirements for the degree of
Master of Applied Science.

Department of Electrical Engineering
Faculty of Science and Engineering
University of Ottawa
Ottawa, Canada
July, 1971.

To my Parents

ABSTRACT

In the design of horn antennas, it is desirable to predict the radiation pattern. The evaluation of the field in the far side and back lobe regions using the aperture method involves difficult surface integrals making the computation tedious. The edge diffraction theory makes this task simpler. A comprehensive analysis for the total E-plane pattern of horn antennas with thick edges using edge diffraction theory has been made in this thesis and an algorithm developed for computing the field pattern to any desired accuracy. This algorithm has been programmed on IBM 360 and the results agree satisfactorily with measured published data.

ACKNOWLEDGEMENTS

The author wishes to express his sincere thanks to Professor A.A.P. de Souza for his guidance, suggestions and encouraging discussions throughout the entire period of research.

A special word of thanks to Miss I. Mayer for the typing assistance.

The author is grateful to the National Research Council of Canada for the financial assistance received through the Research Grants Nos. N.R.C. A 5128 and A 1690.

TABLE OF CONTENTS

CHAPTER I

INTRODUCTION

The microwave region of the electromagnetic spectrum is generally not well defined. However, conventionally the microwave region is usually considered to extend from 0.1 to 25 cm wavelength.

It is known from radiation studies that the minimum scan angle of a radiation system within which the radiation can be confined is directly proportional to the wavelength. When highly directive radiation is desirable the microwave frequencies are used.

At very short wavelenghts, electromagnetic horns provide a simple and convenient means of directing radiation. In a horn antenna several propagating modes are possible. An analytic description of these propagating modes are summarized by Kraus [1].

For the purposes of antenna design, it is desirable to theoretically predict the radiation pattern. For the particular case of aperture antennas, which is studied here, a methodfor the evaluation of the fields has long been known and applied. This is called the aperture method, which provide results for the radiation in the main and the near side lobe regions. In these antennas the field at the edge of the aperture curls around the edge to produce a backward radiation. This radiation can be evaluated in principle by considering the surface currents induced on the outer surface of the radiating system. Since the evaluation of the field involves difficult surface integrals, the computation of the field becomes tedious, if not impossible. Generally, the field pattern in the far side and back-lobe regions is obtained experimentally. However, the application of the edge diffraction theory [2] made it possible to theoretically compute the field pattern in a relatively simple way.

The extension of diffraction concepts developed by Sommerfeld [3] and Pauli [4], who considered the plane wave diffraction by a wedge, provides a method to treat the diffraction of plane and cylindrical waves by thin or thick edges. When this theory is applied to the horn, the total radiation is contributed

by the direct radiation from the source at the horn apex, the diffracted radiation from the edges and the radiation from the images formed at the horn walls due to the reflection of edge diffracted rays.

At higher microwave frequencies, the edge thickness of the practical horn antenna become significant relative to the wavelength used. In this thesis, a comprehensive analysis for the total E-plane pattern of horn antennas with thick edges is made. The algorithm developed permits computation of the field pattern and also to any desired degree of accuracy. This algorithm used on IBM 360 computed the radiation pattern for a sectoral horn antenna. The results obtained are compared with the measured published data available and satisfactory agreement was obtained.

CHAPTER II

REVIEW AND LIMITATIONS OF APERTURE METHOD

The field of an antenna in all regions can be evaluated theoretically by using Schelkunoff's equivalence principle. To apply this method to the case of an aperture antenna, the electric and magnetic currents and fields over the entire surface of the antenna must be determined, which is usually difficult. Further, the computation becomes tedious, if not impossible, when difficult surface integrals are to be evaluated. In the aperture horn antenna the surface currents do not generally contribute significantly to the field in the main lobe and its neighbourhood. The field in this region is primarily due to the Huygen's sources in the antenna aperture [10]. For example, a sectoral horn flared out in the plane of the electric field as shown in Fig. 2.1 is considered.

Let the flare angle be 2Ψ and sufficiently small to make the area of the wave-front approximately equal to the area of the aperture. The field at the plane of the aperture is to be evaluated by considering the antenna to be extending to infinity. By doing so the antenna becomes an infinite horn, and consequently the discontinuity at the plane of the aperture, where the field is evaluated, is removed. It is to be observed that the field will remain constant over the aperture in the y-direction only. But in the x-direction the field varies and depends on the factor $\cos\left(\frac{\pi x_1}{a}\right)$.

At any distant point on the z-axis, the field intensity due to a Huygen's source of intensity E^oH^o will be:

$$\frac{E^o dx\, dy}{2\lambda r}\,(1 + \cos\theta_1) \simeq \frac{E_o\, dx\, dy}{\lambda r} \qquad (2.1)$$

since $\cos\theta_1 \simeq 1$ for distant points in the forward direction. The strengths of the Huygen's sources over the aperature is given by:

$$E^o = E_y^o \cos\frac{\pi x_1}{a} \qquad (2.2)$$

The total field at a distant point on the z-axis is obtained by summing

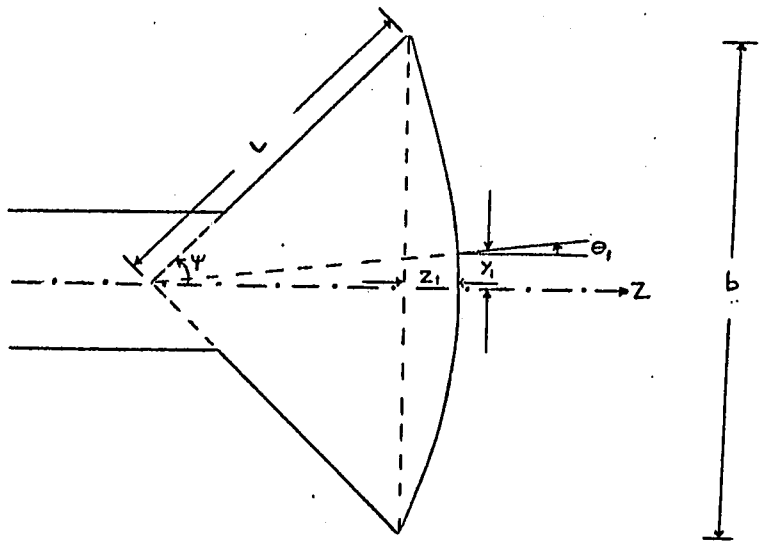

Figure 2.1 An Electromagnetic Horn

the contributions from the Huygen's sources distributed over the wavefront. This can be expressed as:

$$E = \frac{E^o_y}{\lambda r} \int_{-b/2}^{b/2} \int_{-a/2}^{a/2} \cos\frac{\pi x_1}{a} \; e^{j\beta z_1} \; dx_1 \; dy_1 \qquad (2.3)$$

where the reference phase is that due to a source in the plane of the aperture i.e. $z_1 = 0$. From the geometry of Fig 2.1.

$$z_1 = L\cos\theta_1 - L\cos\Psi$$
$$\simeq \frac{b^2}{8L} - \frac{y_1}{2L} \qquad (2.4)$$

Then

$$|E| = \frac{E^o_y}{\lambda r} \int_{-a/2}^{a/2} \cos\frac{\pi x_1}{a} \; dx_1 \left| \int_{-b/2}^{b/2} e^{-j\beta\epsilon} \; dy_1 \right|$$
$$= \frac{4aE^o_y}{\pi\lambda r} \left| \int_o^{b/2} e^{-j\beta\epsilon} \; dy_1 \right| \qquad (2.5)$$

where $$\epsilon = \frac{y_1^2}{2L} \qquad (2.6)$$

Thus it is seen that the aperture method can be used to yield forward fields with good accuracy if the aperture field distribution is known. But the far side lobe and the back lobe region fields connot be obtained in this manner because of the assumptions involved. These fields are generally obtained experimentally until the edge diffraction theory developed by Sommerfeld [3] and Pauli [4] was applied to horn antennas by Russo, Rudduck and Peters [2].

CHAPTER III

EDGE DIFFRACTION THEORY

A. Sommerfeld [3] was the first to succeed in solving the problem of straight edge diffraction by a perfectly conducting wedge. Pauli [4] expressed Sommerfeld's results in an assymptotic series form. The field expression in this form is easier to apply in the analysis of edge diffraction problems. The edge diffraction theory, developed by Sommerfeld and Pauli is briefly summarized here and then applied for the solution of a thick edge horn antenna.

Let a plane electromagnetic wave be normally incident on the wedge of an angle $(2-n)\pi$,as shown in Fig. 3.1. The arrow indicates the direction of the incident wave and the double-arrow indicates the direction of the diffracted wave. By no means is it assumed that n is an integer. The aximuthal angles ψ and ψ_o are the angle of diffraction and the angle of incidence respectively.

If any point P is considered, the field at the point is a solution of the scalar wave equation. The solution of the wave equation necessiates the determination of the boundary values. These are obtained by considering the two possible states of polarization of the incident wave. That is, the electric field vector oscillates perpendicular to the plane of incidence or along this plane. These boundary conditions may be stated as follows.

$$(A)\ u = o \quad ; \quad (B)\ \frac{\partial u}{\partial \tau} = o \tag{3.1}$$

where τ as usual denotes the direction of the normal upon the surface of the wedge. The solution then may be formulated as

$$u(r,\psi) = v(r,\psi+\psi_o) \pm v(r,\psi-\psi_o) \tag{3.2}$$

The right hand side of Eq. (3.2) represents the separation of the total field into the incident and reflected wave.

The polarization determines whether the right hand side is the sum or the difference of two terms. If the electric field vector is perpendicular to the edge, the two terms are summed. When it is parallel to the edge, the difference between the two terms is taken. It is convenient to represent the incident and the reflected fields in the following form.

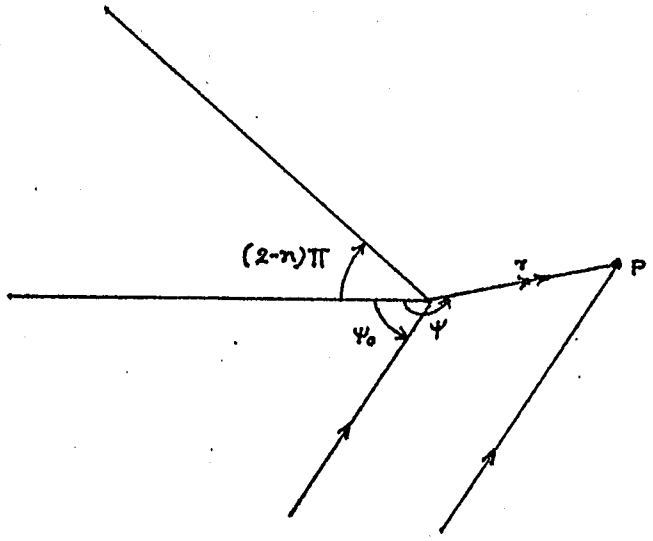

Figure 3.1 Diffraction of a plane wave by a wedge

$$v(r, \phi) = v(r, \Psi \pm \Psi_o) \tag{3.3}$$

Here, the negative sign is associated with the incident field and the positive sign with the reflected field.

The component field is expressed as

$$v(r, \phi) = v^* + v_B \tag{3.4}$$

where v^* is the geometrical optics field and given by

$$v^* = \begin{cases} e^{j\rho \cos(\phi + 2\pi n N)} & -\pi < \phi + 2\pi n N < \pi \\ & N = o, \pm 1, \pm 2, \ldots \\ o & \text{otherwise} \end{cases} \tag{3.5}$$

and v_B, the diffracted field, by

$$v_B = \frac{1}{2\pi n} \int_C \frac{e^{j\rho \cos \beta}}{1 - e^{-j(\beta + \phi)/n}} \, d\beta \tag{3.6}$$

where

$$\rho = kr \tag{3.7}$$

and C represents the appropriate path in the plane of the complex variable.

The assymptotic expression for diffracted field, obtained by Sommerfeld, is given by

$$v_B \simeq (2\pi\rho)^{-1/2} \, e^{-j(\rho + \pi/4)} \, \frac{n^{-1} \sin \frac{\pi}{n}}{\cos \frac{\pi}{n} - \cos \frac{\phi}{n}} \tag{3.8}$$

This expression yields infinite fields in the vicinity of shadow boundary and is therefore valid only if

$$\rho \left(\cos \frac{\pi}{n} - \cos \frac{\phi}{n}\right)^2 >> 1 \tag{3.9}$$

For the special case of n= 2, which represents a zero wedge angle, the diffracted field expression was obtained by Sommerfeld in terms of the Fresnel Integral as

$$v_B(r, \phi) = -e^{j\frac{\pi}{4}} \left(\frac{2}{\pi a}\right)^{1/2} e^{j\rho \cos \phi} \left|\cos \frac{\phi}{2}\right| \int_{(a\rho)^{1/2}}^{\infty} e^{-j\tau^2} \, d\tau \tag{3.10}$$

where $a = 1 + \cos\phi$ (3.11)

and only the positive square root of $(a\rho)$ is to be considered.

By making a transformation of variables and choosing an appropriate contour, Pauli obtained a series expression for Sommerfeld's solution as given below.

$$v_B(r,\phi) = \pi^{-1/2} e^{j\frac{\pi}{4}} \left(\frac{1}{n}\sin\frac{\pi}{n}\right) \times \left\{ \frac{2\left|\cos\frac{\phi}{2}\right|}{\cos\frac{\pi}{n} - \cos\frac{\phi}{n}} e^{jk\rho\cos\phi} \int_{(a\rho)^{1/2}}^{\infty} e^{-j\tau^2} d\tau + \frac{j}{2}(2a)^{-1/2} A_2(\phi) S_1(\rho a) \frac{e^{-jk\rho}}{\rho} + \ldots \right\} \quad (3.12)$$

where

$$A_2(\phi) = (1/4) A_o(\phi) - \frac{1}{n^2} \frac{1+\cos\phi}{\left(\cos\frac{\pi}{n} - \cos\frac{\phi}{n}\right)^2} \cos\frac{\phi}{n} + \frac{2\left[\frac{1}{n}\sin\frac{\phi}{n}\right]^2 (1+\cos\phi) - \left(\cos\frac{\pi}{n} - \cos\frac{\phi}{n}\right)^2}{\left(\cos\frac{\pi}{n} - \cos\frac{\phi}{n}\right)^3} \quad (3.13)$$

$$A_o(\phi) = \frac{1+\cos\phi}{\left(\cos\frac{\pi}{n} - \cos\frac{\phi}{n}\right)} \quad (3.14)$$

$$S_m(\omega) \begin{cases} = -j\,\omega^{-1/2}\left[1 - (m+1/2)(j\omega)^{-1} + \ldots\right] & \text{for } \omega >> 1 \\ \simeq (m-1/2)^{-1}\,\omega^{1/2} & \text{for } \omega \sim o \text{ and } m > o \end{cases} \quad (3.15)$$

For large values of kr, the higher order terms may be neglected, giving

$$v_B(r,\phi) = \frac{2\,e^{j\frac{\pi}{4}}}{n\sqrt{\pi}} \frac{\sin\frac{\pi}{n}\left|\cos\frac{\phi}{2}\right|}{\cos\frac{\pi}{n} - \cos\frac{\phi}{n}} e^{jkr\cos\phi} \int_{(a\rho)^{1/2}}^{\infty} e^{-j\tau^2} d\tau \quad (3.16)$$

The general case of the cylindrical wave diffraction by a wedge can now be discussed, which is relevant to the study and analysis of horn antennas.

Let a line source be located at (x_o, Ψ_o) in the front of a wedge of angle $(2-n)\pi$ as shown in Fig 3.2 (a). Ψ_o is the angle of incidence and Ψ is the angle of diffraction in the direction of the desired field u_a. To relate this discussion with that of the plane wave diffraction, the same symbols and terminology are used.

The plane wave diffraction theory cannot be applied directly to the analysis with cylindrical wave. However, to obtain a solution for u_a the field, the principle of reciprocity is used where the point of observation and source are interchanged, as shown in Fig. 3.2 (b). The fields u_a and u_b are therefore equivalent.

For plane wave incident on the wedge at an angle Ψ, we have

$$u_b = v(x_o, \Psi_o - \Psi) \pm v(x_o, \Psi_o + \Psi) \tag{3.17}$$

Using the property that

$$v(r, \phi) = v(r, -\phi) \tag{3.18}$$

the solution for u_a becomes

$$u_a = v(x_o, \Psi - \Psi_o) \pm v(x_o, \Psi + \Psi_o) \tag{3.19}$$

Eq. (3.19) represents the field at an infinite distance from the edge. But even at moderate distances from the edge, the equation gives a good anglular representation of the field.

It is therefore possible now to view the plane wave diffraction as a special case of the cylindrical wave diffraction with the line source receding to infinity.

The approximated Eq. (3.16), for large $k.r$, is valid for cylindrical wave diffraction.

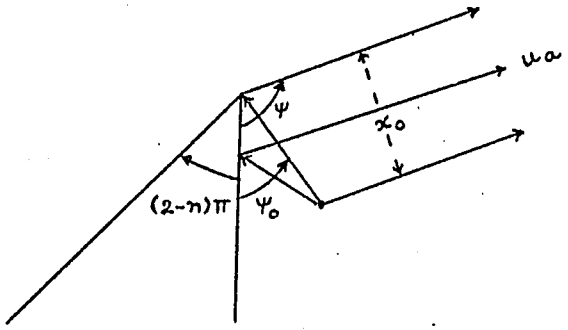

(a)

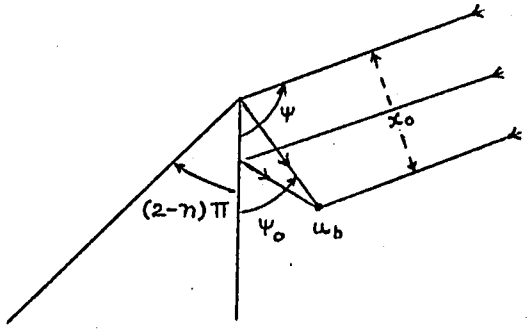

(b)

Figure 3.2 Illustration of Reciprocity

CHAPTER IV

DIFFRACTION BY A THICK EDGE

At higher microwave frequencies, the edge thickness of practical horn antenna becomes significant relative to the wavelength used. For such edges, no methods are available to compute the exact diffracted field. Burke and Keller [5] have formulated a procedure to obtain the diffracted field.

A thick edge is modeled by two 90^{o} wedges as shown in Fig. 4.1. The first order diffracted rays are illustrated in Fig. 4.2. The ray from an arbitrary line source incident on the visible corner X is diffracted into the region of space shown. One of these first order diffracted rays will glide along the surface of the edge and will reach the corner Y. The corner Y, thus illuminated, will in turn diffract rays as shown in the figure. The second order diffracted rays from Y will return to illuminate corner X forming the third order diffraction at corner X. This process of diffraction will continue but the strength of these rays diminish rapidly with each diffraction. Usually only the diffracted rays shown in Fig. 4.2 need be considered for the computation of the field.

Burke and Keller, in their formulation, considered that the field at corner Y, caused by the diffraction at corner X, as equivalent to a plane wave incident at corner Y. But, for edges with thicknesses of the order of a wavelength or less, this concept of plane wave diffraction does not hold. The wave from corner X, illuminating the corner Y, is a cylindrical wave rather than a plane wave. The diffracted fields for the cylindrical wave and the plane wave differ greatly for small edge thicknesses but become nearly the same with increasing edge thickness.

Russo, Rudduck and Peters [2] employed the concept of cylindrical wave diffraction in the case of a thick edge. The illustrations in Fig. 4.3 aid the development of their technique. The thick edge is modeled by a combination of two 90^{o} wedges as before. The point P located at $(x_o, \Psi o)$ represents a line source. The diffracted fields are obtained as discussed earlier. An equivalent source Sx is placed at corner X such that both the original and and equivalent scurces have identical far fields in the direction of the incident ray of Fig. 4.3 (b). Hence, so far

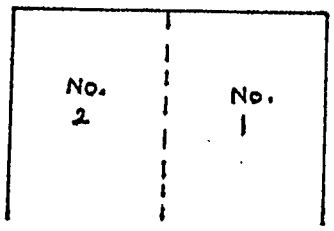

Figure 4.1 The model of a thick edge

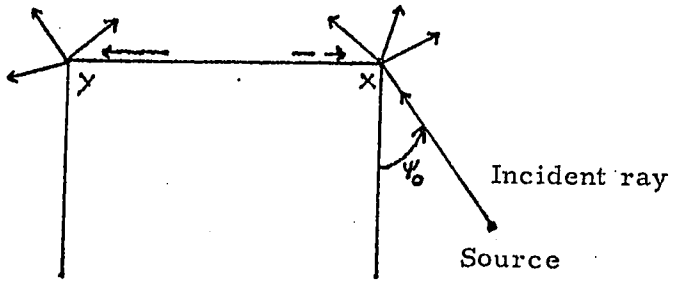

Figure 4.2 Diffraction by a thick edge

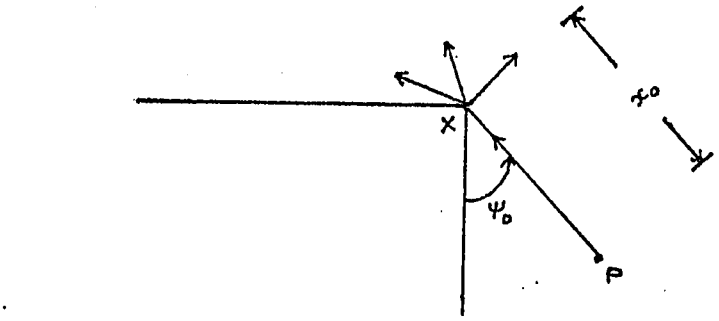

(a)

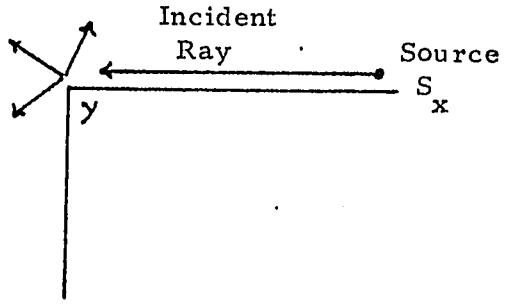

(b)

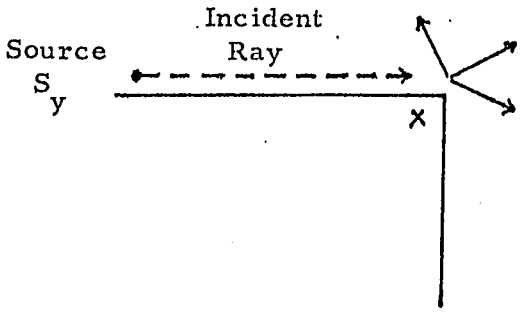

(c)

Figure 4.3 Thick edge diffraction using cylindrical wave concepts

as the illumination of corner Y is concerned, the original source or the equivalent source Sx behave identically. Diffraction at corner Y may now be readily obtained. Now, to obtain the next higher order diffracted field, an equivalent source Sy is located at corner Y as was done in the previous case. This assures the far diffract field of source Sx (caused by corner Y) and the far field of the equivalent source Sy, to be identical in the direction of the incident rays of Fig. 4.3 (c). Clearly either of the sources, Sy or the diffracted field of Sx, causes the same illumination at corner X and with the same intensity. In this manner, multiple diffracted fields of higher orders can be evaluated; but generally they are of neglible magnitude To sum up the contributions of diffractions from corners X and Y, the phase difference between parallel rays from these two corners should be taken into account.

In practical cases, where the width of the edge $d < \lambda/2$, the evaluation of the diffracted field $v_B(r, \phi)$ involves many higher order terms. It has been previously mentioned that $v_B(r, \phi)$ is a very rapidly converging infinite series only when kr is quite large. But for small values of r, the higher order terms do not become neglible and have also to be taken into account with the first term. The rate of convergence then becomes much slower. So, for very small values of edge thickness, the evaluation of $v_B(r, \phi)$ becomes almost impossible. For the case where d=o, n takes on the value 2. This is the special case of a thin edge for which the field $v_B(r, \phi)$ can be evaluated.

CHAPTER V

E- PLANE RADIATION PATTERN OF THICK EDGE HORNS

From the theory of edge diffraction, a powerful method is developed for the evaluation of the radiated field pattern for various kinds of aperature radiating systems. This method has the advantage of facilitating the computation of radiation in the far side and back lobe regions. In this chapter, a comprehensive theoretical analysis based on edge diffraction theory is made. Further an algorithm for the determination of E-plane radiation pattern of horn antennas with significant edge thickness is developed.

The Mechanism of Radiation

The antenna model of Russo, Rudduck and Peters [2] is used in the discussion here. This antenna model consists of a corner reflector formed by two perfectly conducting plane walls intersecting at an angel $2\theta_E$. The antenna is illustrated in Fig. 5.1. The corner reflector is assumed to be infinite in the z-direction which evidently reduces the radiation problem to a two dimensional one. The primary source of radiation is considered to be a magnetic line current placed along the z-axis at the vertex S. This assumption simplifies the treatment in the principal E-plane of the horn antenna fed by a waveguide supporting the TE_{10} mode.

The variation of the field with respect to the azimuthal angle θ is to be evaluate From the Fig. 5.1 it is seen that there are six edges S, A_1, A_2, B_1, B_2 and W in the corner reflector where diffraction occurs. The edges A_1, A_2, B_1 and B_2 have 90° wedge angles. The edges S and W have wedge angles equal to $2\theta_E$ and $2(\pi-\theta_E)$, respectively. Because of the symmetry of the corner reflector, it is enough to carry out the analysis of the upper half of the radiated field only.

A uniform cylindrical wave emanates from the magnetic line source at S and produces the radiated field in the region $-\theta_E \leq \theta \leq \theta_E$. Clearly this wave illuminates the edges A_1 and B_1 generating the first order diffracted waves, which are now directional cylindrical waves. The primary radiation, also called the geometrical optic rays, and the first order diffracted rays are shown in Fig. 5.2.

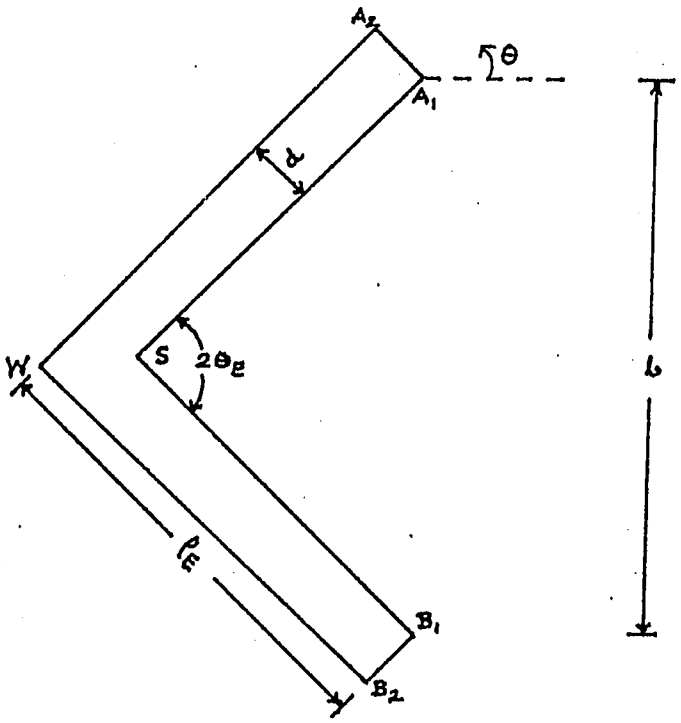

Figure 5.1 The Antenna Model

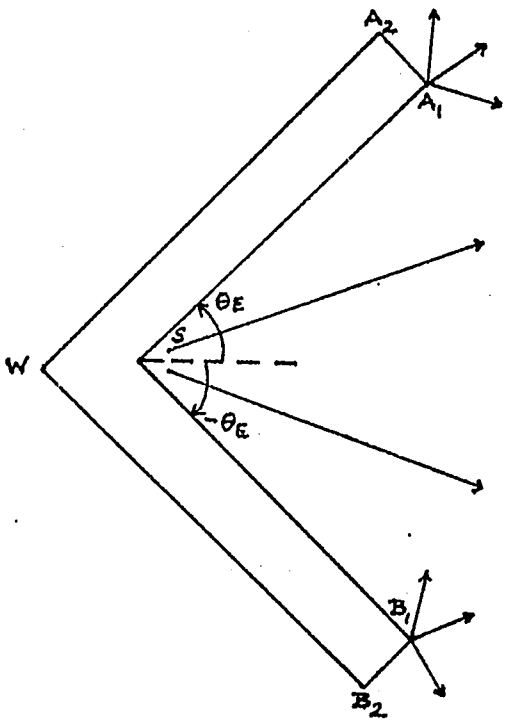

Figure 5.2 Geometrical optic rays and the first order diffractions

The first order diffracted rays emanating from B_1 will now illuminate the edges B_2, A_1 and S to give three second order diffracted waves. Similarly, the first order diffracted wave from A_1 will illuminate edges A_2, B_1 and S to give three more second order diffracted waves. It is to be observed that the diffracted waves from edges A_1 and B_1 do not illuminate edges B_2 and A_2 respectively. This situation has been illustrated in Fig. 5.3.

The second order diffracted rays from S, A_1, A_2, B_1 and B_2 will in turn and in the same manner described above produce the third order diffracted waves. It is also to be observed that the second order diffracted rays from A_2 and B_2 illuminate the edge W which then also generates the third order diffracted rays. This process of illumination and diffraction continue to give the higher order diffracted fields. It is obvious that the induced intensity of illumination becomes weaker as the order of diffraction increases. The phase delay caused by these successive illuminations can be adequately taken into account when the field is computed.

The reflector is assumed to have perfectly conducting walls. Hence, some part of the diffracted waves from A_1 and B_1 are reflected by these walls and contributed to the overall field. From Fig. 5.4 it is seen that the first order diffracted wave from A_1 is reflected by the lower wall. The reflected rays can be studied by using the method of images.

The Fig. 5.5 Shows that one of the first order images in the lower wall illuminates A_1 causing diffraction at that edge. In the same manner, the first order images in the upper wall illuminate B_1 generating a diffracted field. The number of images that are formed in the upper and the lower walls, are obviously determined by the flare angle of the horn $2\theta_E$. Therefore the effect of perfectly conducting walls can be taken into account by using the images formed in them to determine diffracted fields caused by them.

The far field E-plane pattern of the horn antenna can now be computed by superimposing the contributions from the primary geometrical optic rays, the diffraction at the edges S, W, A_1, A_2, B_1 and B_2 and the images formed in the upper and lower walls.

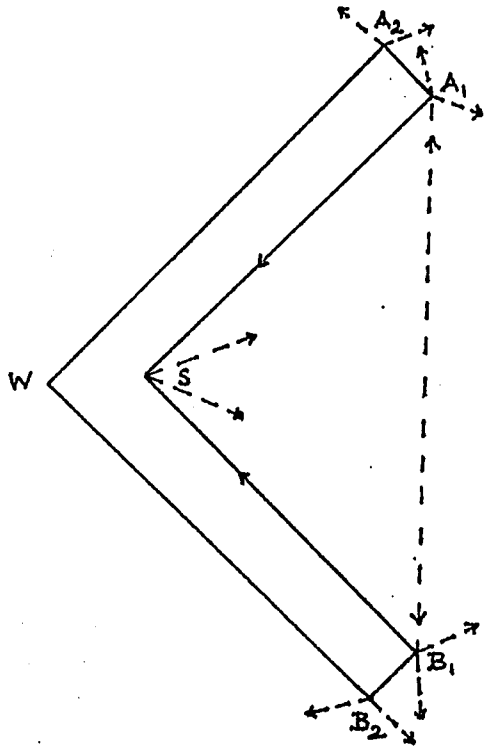

Figure 5.3 Second order diffractions

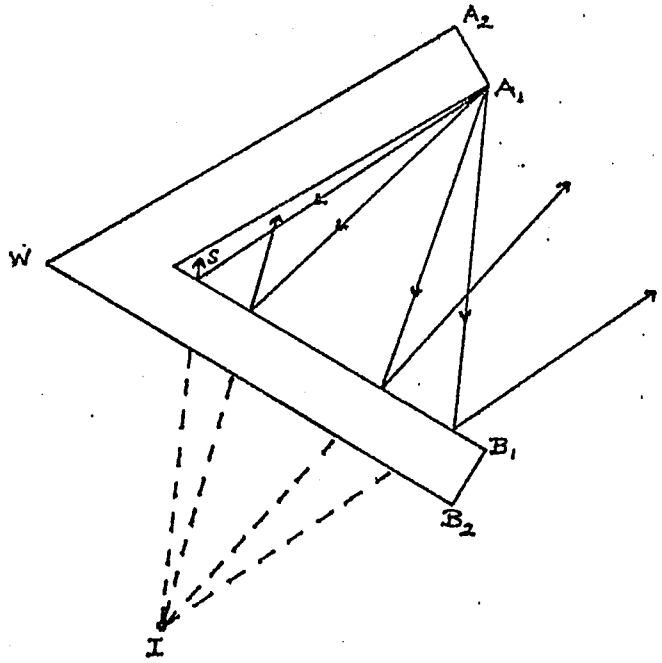

Figure 5.4 Reflection of first order diffracted rays from A_1 by the lower wall

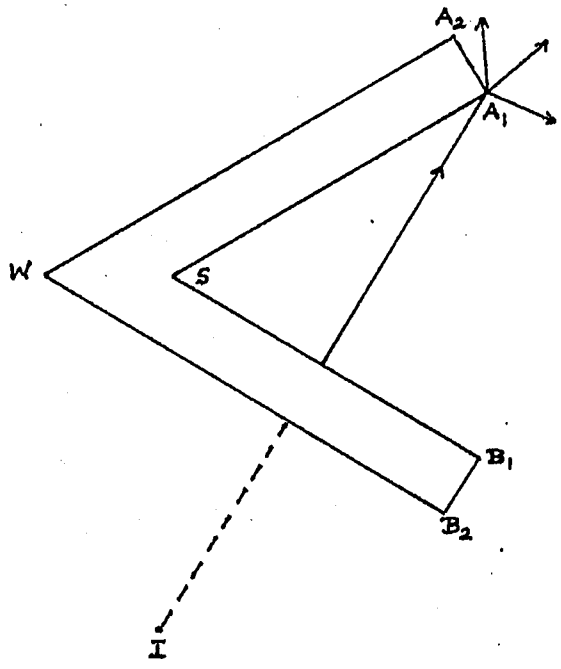

Figure 5.5 Diffraction at A_1 due to one image in the lower wall

Formulation of the Solution in the Infinite Series Form

The uniform cylindrical wave from the line source at vertex S is assumed to be of unit intensity. The far zone diffracted field, contributed by both the incident and reflected waves, is obtained from Eqs. (3.12), (3.13), (3.14) (3.15), (3.16) &(3.19). For convenience the diffracted field, from now onwards, will be denoted by $v_B(r,\phi,n)$ in place of $v_B(r,\phi)$ where the additional parameter n repre the angle of the wedge. It is to be remembered that the cylindrical wave propagation factor $R^{-1/2}$ exp (-j.kR) where R is the distance of the far field point from the source, is suppressed in Eq. (3.19) for convenience.

For the antenna model under study, the results, obtained by Yu and Rudduck [7], in the geometric consideration of the image waves, is used.

The geometric optics rays from the primary source S form a uniform cylindrical wave. In the normalized form, this may be represented as

$$v^*(\theta) = 1, \quad -\theta_E \le \theta \le \theta_E \tag{5.1}$$

where v^* has point S as the phase reference. Edges A_1 and B_1 are illuminated by the cylindrical wave from S with zero angle of incidence as shown in Fig 5.2. Since there is no reflection involved, the diffracted waves from A_1 and B_1 have only one term each. This is easily seen by making reference to Eq. (3.2).

The rays diffracted into the corner reflector will be taken into account later by using the method of images. Excluding these then, the waves directly diffracted to the far field can be written as

$$D^{(1)}_{A_1 S} = v_B(\rho_E, \pi-\theta_E+\theta, 1.5), \quad -\pi/2 \le\theta\le(\pi/2+\theta_E) \tag{5.2}$$

$$D^{(1)}_{B_1 S} = v_B(\rho_E, \pi-\theta_E-\theta, 1.5), \quad \pi/2\ge\theta\ge-(\pi/2+\theta_E) \tag{5.3}$$

where $D_{A_1 S}$ and $D_{B_1 S}$ designate the diffraction at A_1 and B_1 respectively caused by the illumination from the source S. The subscript (1) denotes the first order diffraction. The angles in Eqs. (5.2) and (5.3) may be easily obtained from Fig. 5.1. The argument n is equal to 1.5 for both A_1 and B_1 because both of them have a 90° edge angle. It should be noted that the subscript B in v_B has no relation with edge B_1.

The first order radiation patterns, neglecting the reflections inside

the corner reflector, is readily obtained by suprimposing the terms in Eqs. (5.1), (5.2) and (5.3). The discontinuities of v* at $\theta = \pm \theta_E$ are eliminated by the terms $D_{A_1}S$ and $D_{B_1}S$. But new discontinuities arise in the directions of $\theta = \frac{\pm \pi}{2}$ and $\theta = \pm(\frac{\pi}{2} + \theta_E)$, as illustrated in Fig. 5.1.

The reflection of the first order diffracted wave into the corner reflector is now considered. Since the diffracted waves from A_1 and B_1 are symmetrical with respect to $\theta = o$, the images are formed symmetrically in the lower and upper walls. Using the results of Yu and Rudduck [7], the image waves from the two walls can be obtained by replacing θ of $D_{A_1}S^{(1)}$ and $D_{B_1}S^{(1)}$ in Eqs. (5.2) and (5.3) by $(-2i\theta_E - \theta)$ and $(2i\theta_E - \theta)$ respectively, yielding

$$(I_L^{(1)})_i = v_B [\rho_E, \pi-(2i+1)\theta_E - \theta, 1.5],$$

$$\frac{\pi}{2} - (i+1)\theta_E \leq \theta \leq \frac{\pi}{2} - i\theta_E, \tag{5.4}$$

$$(I_U^{(1)})_i = v_B [\rho_E, \pi - (2i+1)\theta_E + \theta, 1.5]$$

$$-[\frac{\pi}{2} - (i+1)\theta_E] \geq \theta \geq -[\frac{\pi}{2} - i\theta_E] \tag{5.5}$$

$$i = 1, 2, 3, \ldots h$$

and h (the largest integer) $\leq \frac{\pi}{2\theta_E}$

The subscripts L and U denote the image terms from lower and upper walls respectively. The number of images in each wall is equal to the largest integer h which is less than or equal to $\frac{\pi}{2\theta_E}$. When the ratio $\frac{\pi}{2\theta_E}$ is not an integer, the valid region of the last images are modified as

$$\frac{\pi}{2} - (h+1)\theta_E \leq \theta \leq \pi - (2h+1)\theta_E \quad \text{for the lower wall}$$

and $$-[\frac{\pi}{2} - (h+1)\theta_E] \geq \theta \geq -[\pi - (2h+1)\theta_E] \quad \text{for the upper wall}$$

The description of the first order terms has now been completed. The first order radiation pattern can be computed by adding all the above mentioned terms. The second order terms are discussed to yield better accuracy and to

eliminate the discontinuities of the first order radiation pattern.

When $\theta = \frac{\pi}{2}$ the edge A_1 is illuminated by the first order diffracted rays from edge B_1. The intensity of illumination of A_1 due to B_1 is called the first order coupling coefficient. This can be written as:

$$C_{A_1B_1}^{(1)} = D_{B_1S}^{(1)} \quad (\text{at } \theta = \tfrac{\pi}{2}) \tag{5.6}$$

Since the corner reflector has a symmetrical structure, the first order coupling coefficient from A_1 to B_1 in the direction of $\theta = -\frac{\pi}{2}$ is equal to $C_{A_1B_1}^{(1)}$. By using Eqs. (5.2) and (5.3), it is seen that:

$$C_{A_1B_1}^{(1)} = C_{B_1A_1}^{(1)} = v_B(\rho_E, \tfrac{\pi}{2} - \theta_E, 1.5) \tag{5.7}$$

Similarly the edge A_2 is illuminated by the first order diffracted wave from edge A_1 at an angle $\theta = \frac{\pi}{2} + \theta_E$. The edge B_2 is illuminated by the first order diffracted rays from edge B_1 at an angle $\theta = -(\frac{\pi}{2} + \theta_E)$. The corresponding coupling coefficients can be determined in the same way as was described above, i.e.

$$C_{A_2A_1}^{(1)} = C_{B_2B_1}^{(1)} = v_B(\rho_E, \tfrac{3\pi}{2}, 1.5) \tag{5.8}$$

Since the diffracted waves are slowly varying functions in the neighbourhood of a certain angle, it is a good approximation to treat edges A_1, B_1, A_2 and B_2 as illuminated by uniform cylindrical waves of intensities shown in the Eqs. (5.7) and (5.8). With this approximation, the second order diffracted waves can be obtained as

$$D_{A_1B_1}^{(2)} = C_{A_1B_1}^{(1)} [v_B(b, \tfrac{\pi}{2} + \theta, 1.5) + v_B(b, \tfrac{3\pi}{2} - 2\theta_E + \theta, 1.5)]; \quad -\tfrac{\pi}{2} \le \theta \le \tfrac{\pi}{2} + \theta_E; \tag{5.9}$$

$$D_{B_1A_1}^{(2)} = C_{B_1A_1}^{(1)} [v_B(b, \tfrac{\pi}{2} - \theta, 1.5) + v_B(b, \tfrac{3\pi}{2} - 2\theta_E - \theta, 1.5)], \quad \tfrac{\pi}{2} \ge \theta \ge -(\tfrac{\pi}{2} + \theta_E); \tag{5.10}$$

$$D_{A_2A_1}^{(2)} = C_{A_2A_1}^{(1)} [v_B(d, \pi/2 - \theta_E + \theta, 1.5)] \quad -\tfrac{\pi}{2} + \theta_E \le \theta \le \pi + \theta_E; \tag{5.11}$$

$$D_{B_2B_1}^{(2)} = C_{B_2B_1}^{(1)} \left[v_B\left(d, \frac{\pi}{2} - \theta_E - \theta, 1.5\right)\right],$$

$$\frac{\pi}{2} - \theta_E \geq \theta \geq -(\pi + \theta_E); \qquad (5.12)$$

The arguments in the above equations are obtained from Fig. 5.1. The argument n in all the second order diffraction terms stated above is set equal to 1.5 since A_1, A_2, B_1 and B_2 have a 90° wedge angle.

Now it is to be noted that the first order image waves described by Eqs. (5.4) and (5.5) have discontinuities at angles

$$\theta = \pm\left(\frac{\pi}{2} - i\,\theta_E\right), \quad i = 1, 2, 3, \ldots (h-1)$$

At these angles, the edges A_1 and B_1 are illuminated by the rays from images at lower and upper walls respectively. The last images in lower and upper walls for i = h are formed at such positions that they do not illuminate the edges A_1 and B_1. The coupling coefficients from the images to the edge A_1 are obtained from Eq (5.4) as

$$C_{A_1 i}^{(1)} = I_L^{(1)} \left(\text{at } \theta = \frac{\pi}{2} - i\,\theta_E\right), \; i = 1, 2, \ldots (h-1) \qquad (5.13)$$

The coupling coefficients from the images in the upper wall to edge B_1 are, because of the symmetry of the radiating structure, equal to $C_{A_1 i}^{(1)}$. Hence,

$$C_{A_1 i}^{(1)} = C_{B_1 i}^{(1)} = v_B\left[\rho_E, \frac{\pi}{2} - (i+1)\,\theta_E, 1.5\right],$$

$$i = 1, 2, \ldots, (h-1); \qquad (5.14)$$

The second order diffraction at A_1 and B_1, illuminated by the images now become

$$D_{A_1 i}^{(2)} = C_{A_1 i}^{(1)} \left[v_B\left(\rho i, \frac{\pi}{2} + i\,\theta_E + \theta, 1.5\right)\right.$$

$$\left. + v_B\left(\rho i, \frac{3\pi}{2} - (i+2)\,\theta_E + \theta, 1.5\right)\right],$$

$$-\frac{\pi}{2} \leq \theta \leq \frac{\pi}{2} + \theta_E; \qquad (5.15)$$

$$D_{B_1 i}^{(2)} = C_{B_1 i}^{(1)} \left[v_B \left(\rho i, \frac{\pi}{2} + i\,\theta_E - \theta, 1.5 \right) + v_B \left(\rho i, \frac{3\pi}{2} - (i+2)\,\theta_E - \theta, 1.5 \right) \right]$$

$$\frac{\pi}{2} \geq \theta \geq -\left(\frac{\pi}{2} + \theta_E \right); \tag{5.16}$$

where

$$\rho_i = \rho_{i-1} \cos \theta_E + \rho_o \cos i\,\theta_E, \tag{5.17}$$

$$\rho_o = b, \tag{5.18}$$

and

$$i = 1, 2, \ldots, (h-1) \tag{5.19}$$

The second order diffraction terms in Eqs. (5.15) and (5.16) are appropriately arranged for each boundary of the defined regions in Eqs. (5.4) and (5.5). The only exception is the last boundary which is given by

$$\theta = \pm \left[\frac{\pi}{2} - (h+1)\,\theta_E \right], \text{ if } \frac{\pi}{2\theta_E} \text{ is an integer}$$

$$\theta = \pm \left[\frac{\pi}{2} - (2h+1)\,\theta_E \right], \text{ if } \frac{\pi}{2\theta_E} \text{ is not an integer}.$$

The boundaries, in either case, correspond to the directions in which the edge S is illuminated by the induced sources at A_1 and B_1. Therefore the coupling coefficients from A_1 and B_1 to S are obtained from Eqs. (5.4), (5.5) and by symmetry as

$$C_{SA_1}^{(1)} = C_{SB_1}^{(1)} = v_B \left(\rho_E, O, 1.5 \right) \tag{5.20}$$

This coupling gives rise to the second order diffractions at edge S, which are expressed as follows.

$$D_{SA_1}^{(2)} = C_{SA_1}^{(1)} \left[v_B \left(\rho_E, \theta_E - \theta, n_s \right) \right], \quad -\theta_E \leq \theta \leq \theta_E, \tag{5.21}$$

$$D_{SB_1}^{(2)} = C_{SB_1}^{(1)} \left[v_B \left(\rho_E, \theta_E + \theta, n_s \right) \right], \quad -\theta_E \leq \theta \leq \theta_E, \tag{5.22}$$

where

$$n_s = \frac{2\theta_E}{\pi} \tag{5.23}$$

This concludes the descriptions of all second order diffractions which physically take into account the effects of illumination by the first order induced sources. Summing of the second order diffractions at A_1, B_1, A_2, B_2 and S gives,

$$D^{(2)}_{A_1} = D^{(2)}_{A_1B_1} + \sum_{i=1}^{h-1} D^{(2)}_{A_1 i}$$

$$-\frac{\pi}{2} \le \theta \le \frac{\pi}{2} + \theta_E; \qquad (5.24)$$

$$D^{(2)}_{B_1} = D^{(2)}_{B_1 A_1} + \sum_{i=1}^{h-1} D^{(2)}_{B_1 i},$$

$$\pi/2 \ge \theta \ge -(\pi/2 + \theta_E); \qquad (5.25)$$

$$D^{(2)}_{A_2} = D^{(2)}_{A_2 A_1},$$

$$-\pi/2 + \theta_E \le \theta \le \pi + \theta_E; \qquad (5.26)$$

$$D^{(2)}_{B_2} = D^{(2)}_{B_2 B_1},$$

$$-\pi/2 - \theta_E \ge \theta \ge -(\pi + \theta_E); \qquad (5.27)$$

$$D^{(2)}_{S} = D^{(2)}_{SA_1} + D^{(2)}_{SB_1},$$

$$-\theta_E \le \theta \le \theta_E. \qquad (5.28)$$

Following the same procedure used to obtain equations (5.4) and (5.5), the second order image waves from the lower and upper walls are expressed as

$$(I^{(2)}_L)_i = C^{(1)}_{A_1B_1} [v_B(b, \pi/2 - 2i\theta_E - \theta, 1.5) + v_B(b, 3\pi/2 - 2(i+1)\theta_E - \theta, 1.5)]$$
$$+ \sum_{K=1}^{h-1} C^{(1)}_{A_1K} [v_B(\rho_K, \pi/2 - i\theta_E - \theta, 1.5) + v_B(\rho_K, 3\pi/2 - (3i+2)\theta_E - \theta, 1.5)]$$

$$\pi/2 - (i+1)\theta_E \le \theta \le \pi/2 - i\theta_E; \qquad (5.29)$$

$$(I_U^{(2)})_i = C_{B_1A_1}^{(1)} \left[v_B(b, \pi/2 - 2i\theta_E + \theta, 1.5) + v_B(b, 3\pi/2 - 2(i+1)\theta_E + \theta, 1.5) \right] + \sum_{K=1}^{h-1} C_{B_1K}^{(1)} \left[v_B(\rho_K, \pi/2 - i\theta_E + \theta, 1.5) + v_B(\rho_K, 3\pi/2 - (3i+2)\theta_E + \theta, 1.5) \right],$$

$$-[\pi/2 - (i+1)\theta_E] \geq \theta \geq -[\pi/2 - i\theta_E]; \qquad (5.30)$$

and $$i = 1, 2, 3, \ldots h \qquad (5.31)$$

The second-order image terms described above are readily obtained by replacing θ of $D_{A_1}^{(2)}$ and $D_{B_1}^{(2)}$ by $(\mp 2i\theta_E - \theta)$, respectively. It should be noted here that the boundary of the last image, where i = h, depends on whether $\pi/2\theta_E$ is exactly an integer or not. If $\pi/2\theta_E$ is an integer, then these boundaries are obtained from equations (5.29) and (5.30). Otherwise, these have to be calculated in the same manner as was done for first order images.

This concludes the description of the second order diffraction and the image terms. Theoretically it is possible to calculate the third and higher order terms. But for all practical purposes, the contributions of the terms of order three or more to the field are negligibly small. However, for completeness the iterative formulas for all possible orders of difraction and image are presented below:

$$D_{A_1}^{(m)}(\theta) = D_{A_1S}^{(m)} + D_{A_1B_1}^{(m)} + D_{A_1A_2}^{(m)} + \sum_{i=1}^{h-1} D_{A_1i}^{(m)} \qquad (5.32)$$

$$D_{B_1}^{(m)}(\theta) = D_{B_1S}^{(m)} + D_{B_1A_1}^{(m)} + D_{B_1B_2}^{(m)} + \sum_{i=1}^{h-1} D_{B_1i}^{(m)} \qquad (5.33)$$

$$D_{A_2}^{(m)}(\theta) = D_{A_2A_1}^{(m)} + D_{A_2W}^{(m)}, \qquad (5.34)$$

$$D_{B_2}^{(m)}(\theta) = D_{B_2B_1}^{(m)} + D_{B_2W}^{(m)}, \qquad (5.35)$$

$$D_S^{(m)}(\theta) = D_{SA_1}^{(m)} + D_{SB_1}^{(m)}, \qquad (5.36)$$

$$D_W^{(m)}(\theta) = D_{WA_2}^{(m)} + D_{WB_2}^{(m)}, \qquad (5.37)$$

$$(I_L^{(m)})_i = D_{A_1}^{(m)}(-2i\theta_E - \theta), \tag{5.38}$$

and $$(I_U^{(m)})_i = D_{B_1}^{(m)}(2i\theta_E - \theta), \tag{5.39}$$

where $$D_{A_1S}^{(m)}(\theta) = C_{A_1S}^{(m-1)}[v_B(\rho_E, \pi - \theta_E + \theta, 1.5)],$$

$$-\pi/2 \le \theta \le \pi/2 + \theta_E; \tag{5.40}$$

$$D_{B_1S}^{(m)}(\theta) = D_{A_1S}^{(m)}(-\theta), \ \pi/2 \ge \theta \ge -(\pi/2 + \theta_E); \tag{5.41}$$

$$D_{A_1B_1}^{(m)}(\theta) = C_{A_1B_1}^{(m-1)}[v_B(b, \pi/2 + \theta, 1.5) + v_B(b, \tfrac{3\pi}{2} - 2\theta_E + \theta, 1.5)],$$

$$-\pi/2 \le \theta \le \pi/2 + \theta_E; \tag{5.42}$$

$$D_{B_1A_1}^{(m)}(\theta) = D_{A_1B_1}^{(m)}(-\theta), \ \pi/2 \ge \theta \ge -(\pi/2 + \theta_E); \tag{5.43}$$

$$D_{A_1A_2}^{(m)}(\theta) = C_{A_1A_2}^{(m-1)}[v_B(d, \pi/2 + \theta_E - \theta, 1.5)],$$

$$-\pi/2 \le \theta \le \pi/2 + \theta_E; \tag{5.44}$$

$$D_{B_1B_2}^{(m)}(\theta) = D_{A_1A_2}^{(m)}(-\theta), \ \pi/2 \ge \theta \ge -(\pi/2 + \theta_E); \tag{5.45}$$

$$D_{A_2A_1}^{(m)}(\theta) = C_{A_2A_1}^{(m-1)}[v_B(d, \pi/2 - \theta_E + \theta, 1.5)],$$

$$-\pi/2 + \theta_E \le \theta \le \pi + \theta_E \tag{5.46}$$

$$D_{B_2B_1}^{(m)}(\theta) = D_{A_2A_1}^{(m)}(-\theta), \ \pi/2 - \theta_E \ge \theta \ge -(\pi + \theta_E); \tag{5.47}$$

$$D_{A_2W}^{(m)}(\theta) = C_{A_2W}^{(m-1)}[v_B(\rho_E, \pi + \theta_E - \theta, 1.5)],$$

$$-\pi/2 + \theta_E \le \theta \le \pi + \theta_E; \tag{5.48}$$

$$D_{B_2W}^{(m)}(\theta) = D_{A_2W}^{(m)}(-\theta), \ \pi/2 - \theta_E \ge \theta \ge -(\pi + \theta_E); \tag{5.49}$$

$$D_{SA_1}^{(m)}(\theta) = C_{SA_1}^{(m-1)}[v_B(\rho_E, \theta_E - \theta, n_s)],$$

$$-\theta_E \le \theta \le \theta_E; \tag{5.50}$$

$$D_{SB_1}^{(m)}(\theta) = D_{SA_1}^{(m)}(-\theta), \ -\theta_E \le \theta \le \theta_E; \tag{5.51}$$

$$D_{WA_2}^{(m)}(\theta) = C_{WA_2}^{(m-1)} \left[v_B(\rho_E, -\theta_E + \theta, n_W) \right], \quad \theta_E \le \theta \le 2\pi - \theta_E; \tag{5.52}$$

$$D_{WB_2}^{(m)}(\theta) = D_{WA_2}^{(m)}(-\theta), \; -\theta_E \ge \theta \ge -(2\pi - \theta_E); \tag{5.53}$$

$$D_{A_1 i}^{(m)}(\theta) = C_{A_1 i}^{(m-1)} \left[v_B(\rho_i, \pi/2 + i\theta_E + \theta, 1.5) + v_B(\rho_i, \frac{3\pi}{2} - (i+2)\theta_E + \theta, 1.5) \right], \quad -\pi/2 \le \theta \le \pi/2 + \theta_E; \tag{5.54}$$

$$D_{B_1 i}^{(m)}(\theta) = D_{A_1 i}^{(m)}(-\theta), \; \pi/2 \ge \theta \ge -(\pi/2 + \theta_E); \tag{5.55}$$

The property of symmetry of the pattern about $\theta = o$ has been used to obtain symmitrical terms. The coupling coefficients are expressed as

$$C_{A_1 S}^{(m)} = D_S^{(m)}(\theta = \theta_E); \tag{5.56}$$

$$C_{A_1 B_1}^{(m)} = D_{A_1}^{(m)}(\theta = -\pi/2); \tag{5.57}$$

$$C_{A_1 A_2}^{(m)} = D_{A_2}^{(m)}(\theta = -\pi/2 + \theta_E); \tag{5.58}$$

$$C_{A_2 A_1}^{(m)} = D_{A_1}^{(m)}(\theta = \pi/2 + \theta_E); \tag{5.59}$$

$$C_{A_2 W}^{(m)} = D_W^{(m)}(\theta = \theta_E); \tag{5.60}$$

$$C_{SA_1}^{(m)} = D_{A_1}^{(m)}(\theta = -\theta_E); \tag{5.61}$$

$$C_{WA_2}^{(m)} = D_{A_2}^{(m)}(\theta = \pi + \theta_E); \tag{5.62}$$

$$C_{A_1 i}^{(m)} = D_{A_1}^{(m)}(\theta = -\pi/2 - i\theta_E); \tag{5.63}$$

The total far field pattern of the horn antenna can now be calculated by the super-

position of all terms in the iterative formulas developed. Taking the edge A_1 as the common phase reference and considering only the upper half region, that is $o \leq \theta \leq \pi$, the total E- plane far field $u_F(\theta)$ is given by the expression

$$u_F(\theta) = \left[v^* + \sum_{m=2}^{\infty} D_s^{(m)}\right] Y_{A_1 S} + \left[\sum_{m=1}^{\infty} D_{A_1}^{(m)}\right] + \left[\sum_{m=1}^{\infty} D_{B_1}^{(m)}\right] Y_{A_1 B_1} + \left[\sum_{m=2}^{\infty} D_{A_2}^{(m)}\right] Y_{A_1 A_2} + \left[\sum_{m=2}^{\infty} D_{B_2}^{(m)}\right] Y_{A_1 B_2} + \left[\sum_{m=3}^{\infty} D_W^{(m)}\right] Y_{A_1 W} + \sum_{i=1}^{h} \left[\sum_{m=1}^{\infty} (I_L^{(m)})_i\right] Y_{A_1 i} + \left[\sum_{m=1}^{\infty} (I_u^{(m)})_h\right] Y_{B_1 h} Y_{AB} \quad (5.64)$$

The last images in the upper wall are included because, in general, they contribute to the radiation in the upper half region. The Y's are the local phase factors. Each of the Y terms represent the phase difference between a ray from edge A_1 and a ray parallel to that emanating from the source denoted by the second variable. These are written as

$$Y_{A_1 S} = \exp\left[-j2\pi\rho_E \cos(-\theta_E + \theta)\right], \quad (5.65)$$

$$Y_{A_1 B_1} = \exp\left[-j\, 2\,\pi b \sin\theta\right], \quad (5.66)$$

$$Y_{A_1 A_2} = \exp\left[-j\, 2\pi d \,\mathrm{Sin}\,(\theta_E - \theta)\right], \quad (5.67)$$

$$Y_{A_1 B_2} = \exp\left[-j\, 2\pi(b \sin\theta + d \sin(\theta_E + \theta))\right], \quad (5.68)$$

$$Y_{A_1 W} = \exp\left[-j\, 2\pi\,(\rho_E \cos(\theta_E - \theta) + d \sin(\theta_E - \theta))\right], \quad (5.69)$$

$$Y_{A_1 i} = \exp\left[-j\, 2\pi\rho_i \sin(i\,\theta_E + \theta)\right], \quad (5.70)$$

and

$$Y_{Bh} = \exp\left[-j2\,\pi\rho_i \sin(h\,\theta_E - \theta)\right], \quad (5.71)$$

CHAPTER VI

DISCUSSION OF RESULTS

In the previous chapter, the total E-plane far field $u_F(\theta)$ was given by Eq.(5.64). The terms in this equation represent the direct, diffracted and image fields. It is to be noted that in the first term the summation runs from m=2 to m=∞ corresponding to the second and higher order diffracted fields from the edge S because there is no first order diffraction from that edge. But the second term represents edge A_1 where the summation is from m=1 to m=∞ since first and higher order diffraction occurs at this edge. The third term corresponding to edge B_1 and the last two terms due to the images also have m running from 1 to ∞ expressing the first and higher order diffractions and first and higher order images respectively. The fourth and the fifth terms due to edges A_2 and B_2 represent second and higher order diffractions at these edges. The term corresponding to edge W is the sixth term where the summation begins from m=3 because of the absence of first and second order diffraction effects.

For the purpose of computation of the E-plane far field of the thick edge horn, higher order diffraction terms are neglected. For the source, all the diffraction terms are small to appreciably influence the accuracy of the computations made. This is because the wave has to travel the slant length of the horn from the edge A_1 to be diffracted at the source S. For edges A_1, B_1, A_2, and B_2 the second order diffractions have been taken into account. But for edges A_1 and B_1 only, the third order diffraction is considered. It is only at these two edges, because of the small distances A_2A_1 and B_2B_1, the third order becomes appreciable. All other third order diffraction terms are neglected. In the last two image terms, only the first order images are considered. The diffraction at edges A_1 and B_1 due to the images are also neglected.

The thick edge of the horn antenna is simulated by considering a 0.5 inch width strip around and perpendicular to the rim of the horn as illustrated in Fig. 6.1a. The thickness of this strip is considered negligible relative to the wave

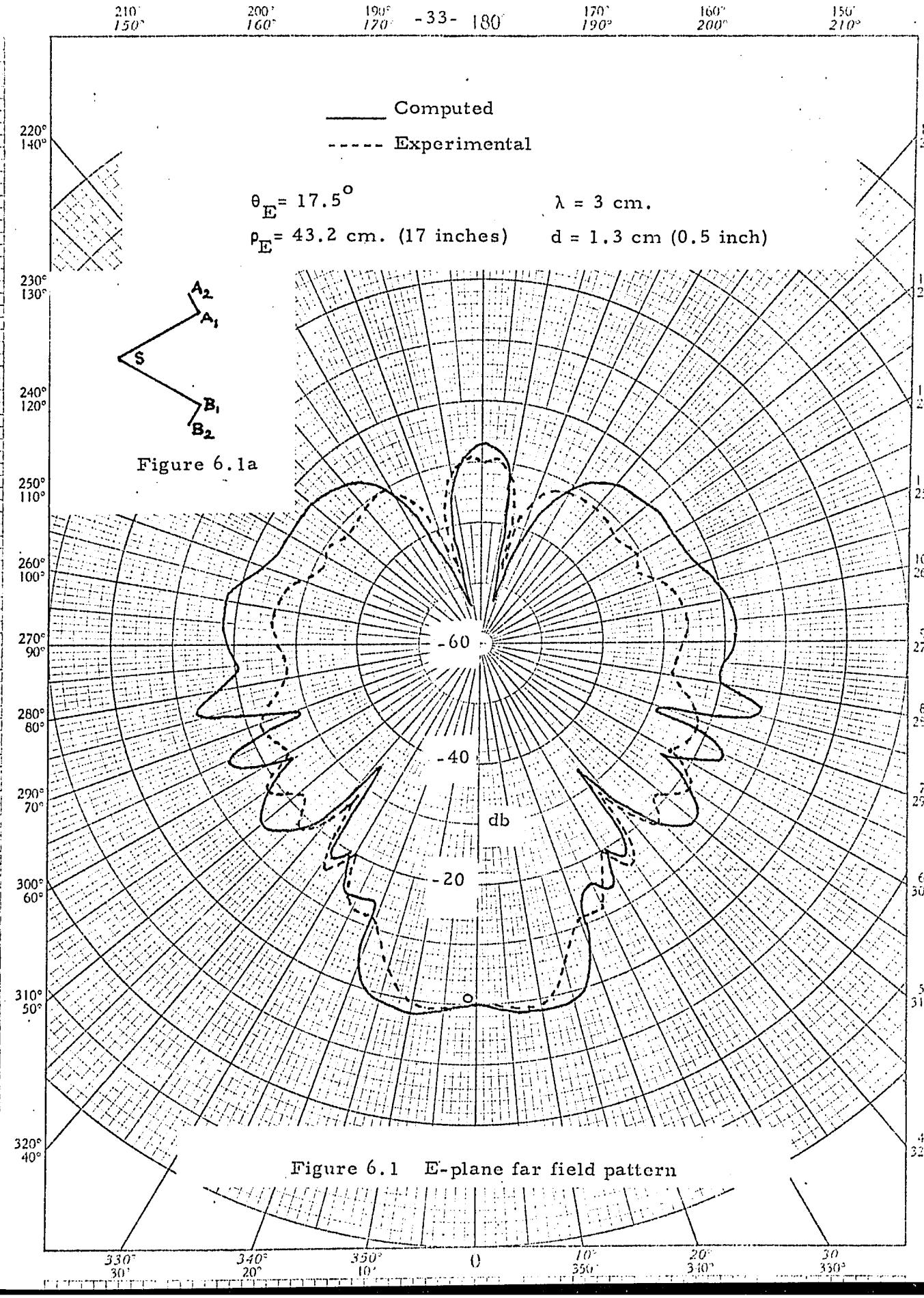

Figure 6.1a

Figure 6.1 E-plane far field pattern

length used. The diffracted field due to A_2 is reflected by the body of the horn and this is taken into account by the method of images.

The E-plane far field pattern is plotted in Figs. 6.1, 6.2, 6.3, and 6.4. In Fig. 6.1 the computed and published experimental [2] curves are plotted for comparison. The parameters and the wavelength are indicated on the graph. It is clearly seen that in general good agreement between the curves has been achieved. However, there are some deviation observed between the computed and experimental curves in the far side lobe regions and in the neighbourhood of 15°. It must be borne in mind that the assymptotic expression used for the diffracted field is only approximate since only a finite number of terms are considered. Further, the expression itself becomes less accurate in the shadow boundary regions. In the horn considered here, the shadow boundary regions are about 17.5° and 107.5°. The field in the 107.5° boundary region, it is to be noted, is caused after the direct radiation from the horn apex is diffracted twice at edges A_1 and A_2. The error involved in approximating the diffracted field by the analytic expression becomes cumulative after each diffraction. The deviation in 107° region may be thus explained.

In order to study the influence of the parameters in the geometry of the horn, several radiation patterns were computed for different values of parameters. In each of the Figs. 6.2, 6.3 and 6.4, the flare angle is held constant and the frequency is changed. From the radiation patterns, the following observations are made. As the flare angle increases, the width of the forward lobe increases which is anticipated. Moreover, the back lobe radiation generally decreases with increasing flare angles, because of a larger forward radiation. But studying each of the figures separately, it can be infered that as the wavelength increases the back lobe radiation increases. This phenomenon is anticipated because the dimensions of the horn become smaller relative to the wavelength consequently inducing more curling around the edge.

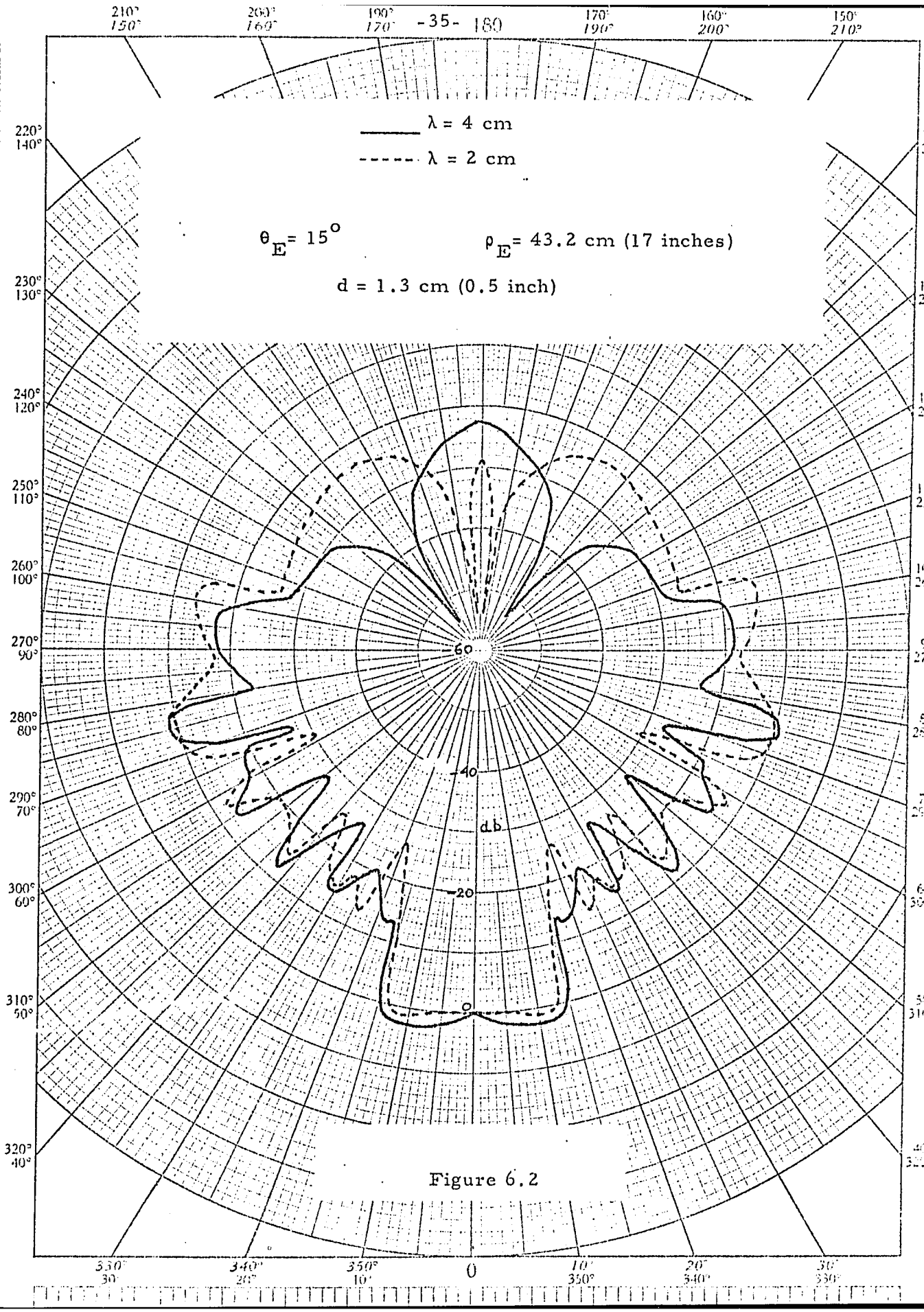

Figure 6.2

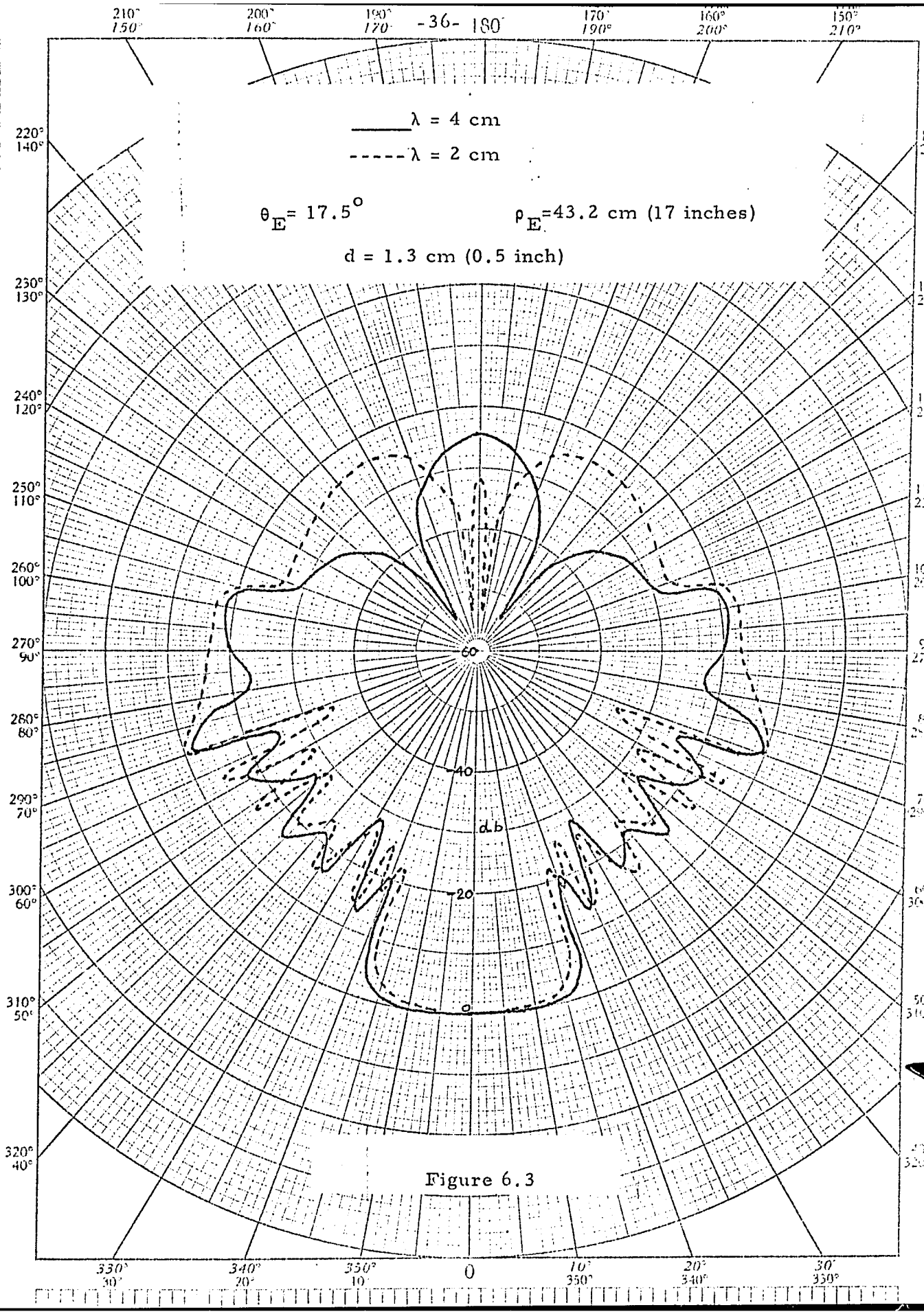
λ = 4 cm
λ = 2 cm
θE= 17.5°
ρE=43.2 cm (17 inches)
d = 1.3 cm (0.5 inch)
60
40
20
0
db
180
0
KEUFFEL & ESSER CO.

Figure 6.3

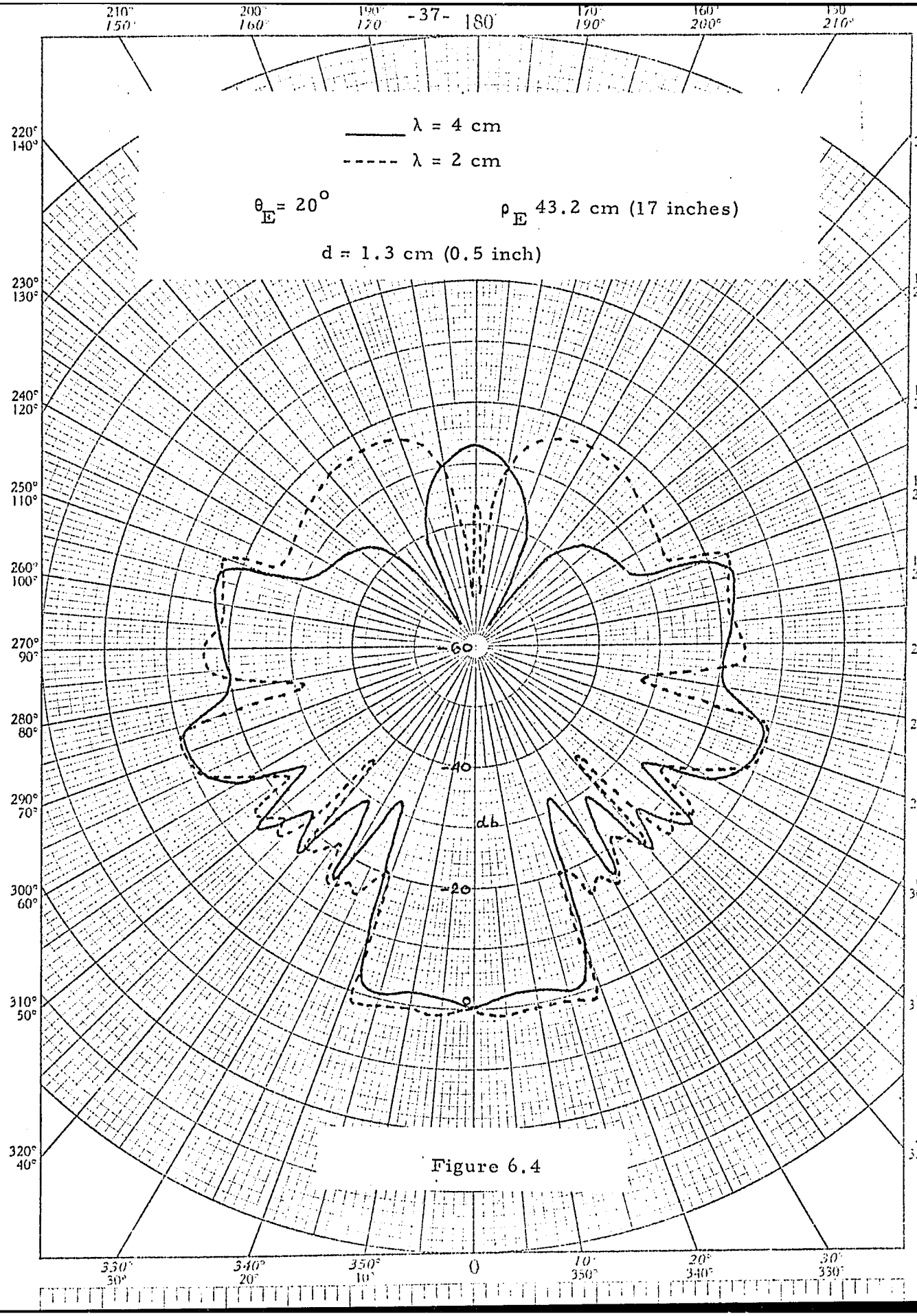
λ = 4 cm
λ = 2 cm
θ_E = 20°
ρ_E 43.2 cm (17 inches)
d = 1.3 cm (0.5 inch)
-60
-40
-20
0
db

Figure 6.4

Bibliography

[1] J. D. Kraus, Antennas, McGraw-Hill Book Co., Inc., 1950, pp. 375-380.

[2] P. M. Russo, R. C. Rudduck and L. Peters, "A Method for Computing E-Plane Patterns of Horn Antennas," IEEE Transactions on Antennas and Propagation, vol. AP-13. pp 219-224, March 1965.

[3] A. Sommerfeld, Optics, New York: Academic Press, Inc., 1954, pp. 245-265.

[4] W. Pauli, "On Asymptotic Series for Functions in the Theory of Diffraction of Light", Physical Review, vol. 54, pp. 924-931, December 1938.

[5] J. E. Burke and J. B. Keller, "Diffraction by a thick screen, a step related axially symmetric objects", EDL-E48, Contract DA 36-039-sc-78281, Sylvania Electronic Systems, Mountain View, Calif., March 1960.

[6] J. S. Yu, R. C. Rudduck and L. Peters, Jr., "Comprehensive Analysis for E-Plane of Horn Antennas by Edge Diffraction Theory", IEEE Transactions on Antennas and Propagation, vol. AP-14, pp. 138-149, March 1966.

[7] J. S. Yu and R. C. Rudduck, "The E-plane radiation pattern of an antenna model for horn antennas", Antenna Lab., The Ohio State University Research Foundation, Columbus, Rept. 1767-3, April 1, 1965.

[8] E. V. Jull, "Edge Diffraction Theory In Antenna Calculation", Bulletin of the Radio and Electrical Engineering Division, National Research Council of Canada, vol. 21, no. 1, January-March, 1971.

[9] S. Silver, Microwave Antenna Theory and Design, New York: Dover Publications, Inc., Chapter 10.

[10] E. C. Jordan, Electromagnetic Waves and Radiating Systems, Constable and Co., Ltd., pp. 577-579.

VITA

Name: Asoknath Chattopadhyay

Born: Jamshedpur, India, Feb. 10, 1947.

Education:

Secondary: Serampore Union Institution, West Bengal, India.

University: St. Xavier's College,
University of Calcutta,
B.Sc. with Honors in Physics, 1965.

Institute of Radio Physics and Electronics,
University of Calcutta.
B.Tech., 1967
M. Tech., 1968.